# Electronic Supplemental information

## Self-templated flower-like NiCoZn-carbonate hydroxides hollow nanospheres for asymmetric supercapacitors with high performance

Rongrong Liu[a], Xin Gao[a], Yanqiu Xie[a], Qinhan Liu[a], Kai Zhang[a], Yijia Sun[a], He Bai[a], Fei Yao[b] and Hongyan Yue*[a]

[a] School of Materials Science and Chemical Engineering, Harbin University of Science and Technology, Harbin 150040, People's Republic of China

[b] Department of Materials Design and Innovation, University at Buffalo, North Campus, Buffalo 14260, USA

*Corresponding author:

Prof. Hongyan Yue

School of Material Science and Chemical Engineering,

Harbin University of Science and Technology,

Harbin 150040, People's Republic of China.

Tel: +86-451-86392258

Email: hyyue@hrbust.edu.cn

## Evaluation of electrochemical measurements

The gravimetric specific capacitance of a single electrode in a three-electrode system was calculated from the GCD curve according to the following equation:

$$C = \frac{I \times \Delta t}{m \times \Delta V}$$

(1)

Where $C$ is the specific capacitance (F g$^{-1}$), $I$ is the discharge current (A), $\Delta t$ is the discharge time (s), $m$ is the mass of active material (g).

The specific capacitance of the asymmetric capacitor in a two-electrode system was obtained by the following equation:

$$C = \frac{I \times \Delta t}{M \times \Delta V}$$

(2)

Where $C$ is the specific capacitance (F g$^{-1}$), $M$ is the total mass of the positive and negative electrodes (g).

According to the charge matching principle, the optimal mass ratio of Ni$_1$Co$_1$Zn$_{0.25}$-CH to AC is 1:3.57 to assemble asymmetric supercapacitors.

$$q_{+} = q_{-}$$

(3)

$$q = mCV$$

(4)

$$\frac{m_{+}}{m_{-}} = \frac{C_{-} \times V_{-}}{C_{+} \times V_{+}}$$

(5)

Where $q$ is the electrode charge, $m_{+}/m_{-}$ is the mass of the positive/negative active material (g), $C_{+}/C_{-}$ is the specific capacitance of the positive/negative material, $V_{+}/V_{-}$ is the voltage window of the positive/negative electrode.
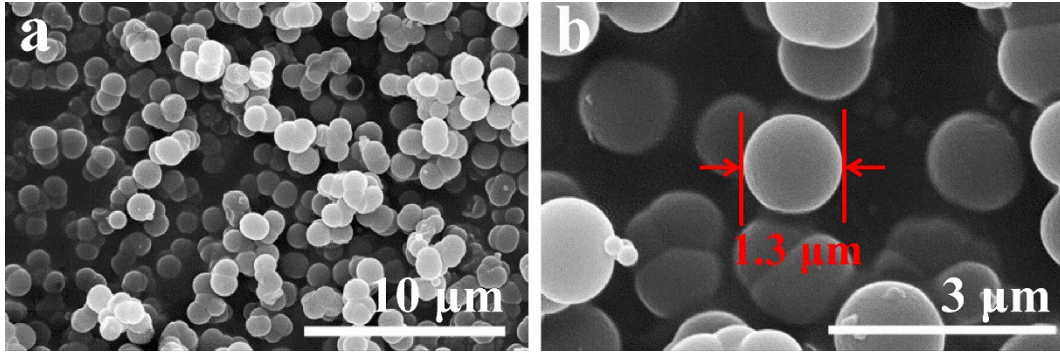
The power density (P) and the energy density (E) are calculated as follows:

$$E = \frac{C \times V^2}{2 \times 3.6}$$

(6)

$$P = \frac{3600 \times E}{\Delta t}$$

(7)

**Fig. S1.** SEM images of $Ni_1Co_1Zn_{0.25}$-G prepared without the addition of PVP (K30) at different magnifications. **a**, low magnification. **b**, high magnification.

Fig. S1 shows SEM images of $Ni_1Co_1Zn_{0.25}$-G prepared without the addition of PVP (K30) at different magnifications. It can be seen that $Ni_1Co_1Zn_{0.25}$-G prepared without the addition of PVP (K30) is a ball-shape with a diameter of about 1.3 μm, which are not completely uniform and some balls connect together.
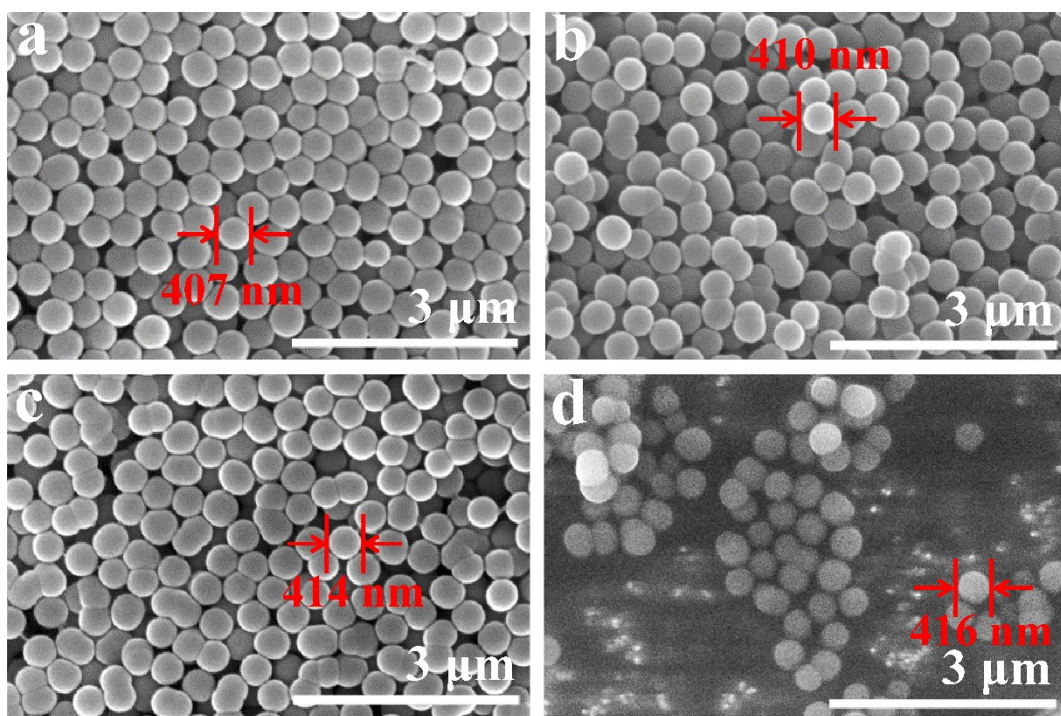
**Fig. S2.** SEM images of NiCoZn-G prepared with different additions of $Zn^{2+}$. **a**, $Ni_1Co_1Zn_0$-G. **b**, $Ni_1Co_1Zn_{0.25}$-G. **c**, $Ni_1Co_1Zn_{0.5}$-G. **d**, $Ni_1Co_1Zn_1$-G.
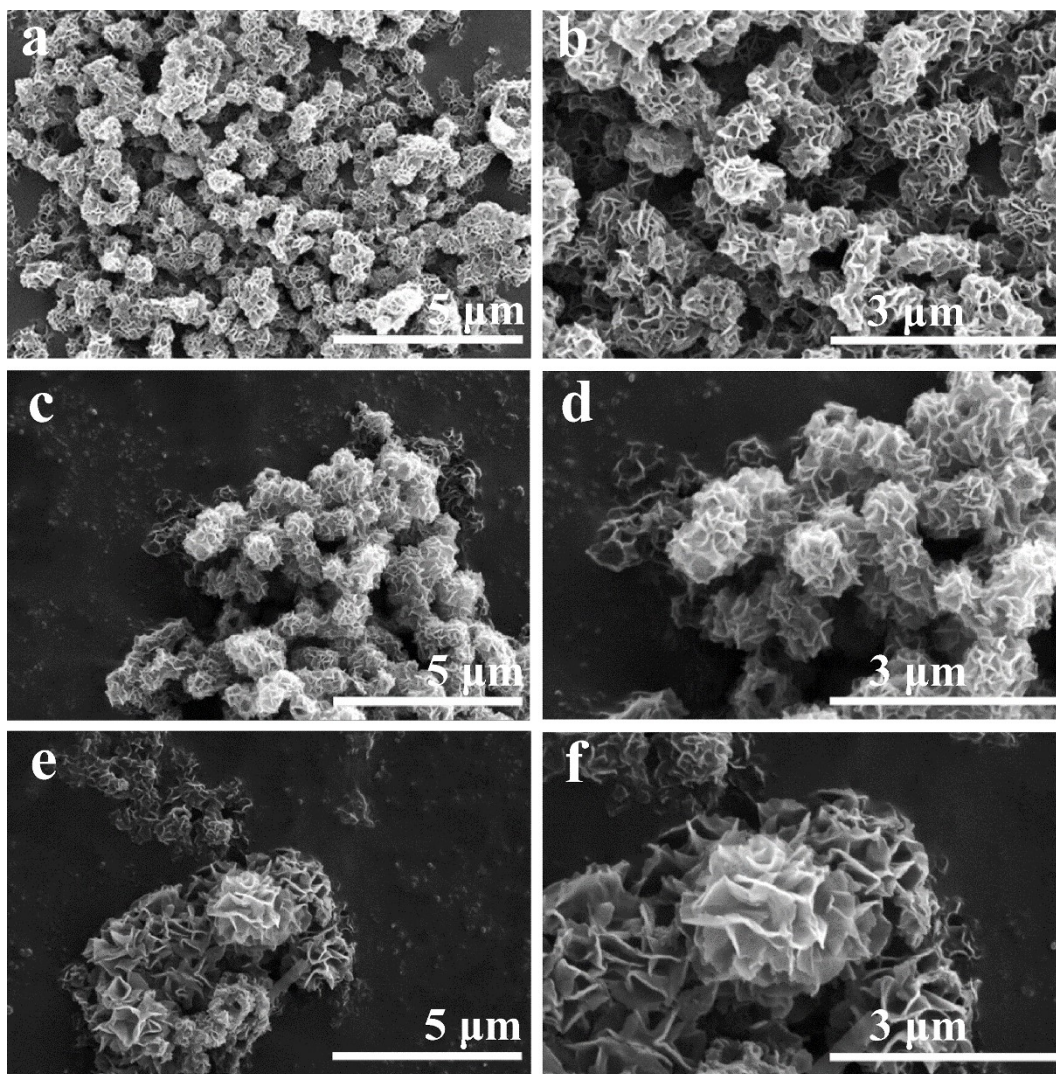
SEM images of NiCoZn-G prepared with different additions of $Zn^{2+}$ are shown in Fig. S2. The results indicate that NiCoZn-G prepared by the solvothermal reaction with different additions of $Zn^{2+}$ is uniform and well dispersed with a diameter of about 400 nm, indicating that PVP (K30) plays the role of a stabilizer and size control agent.
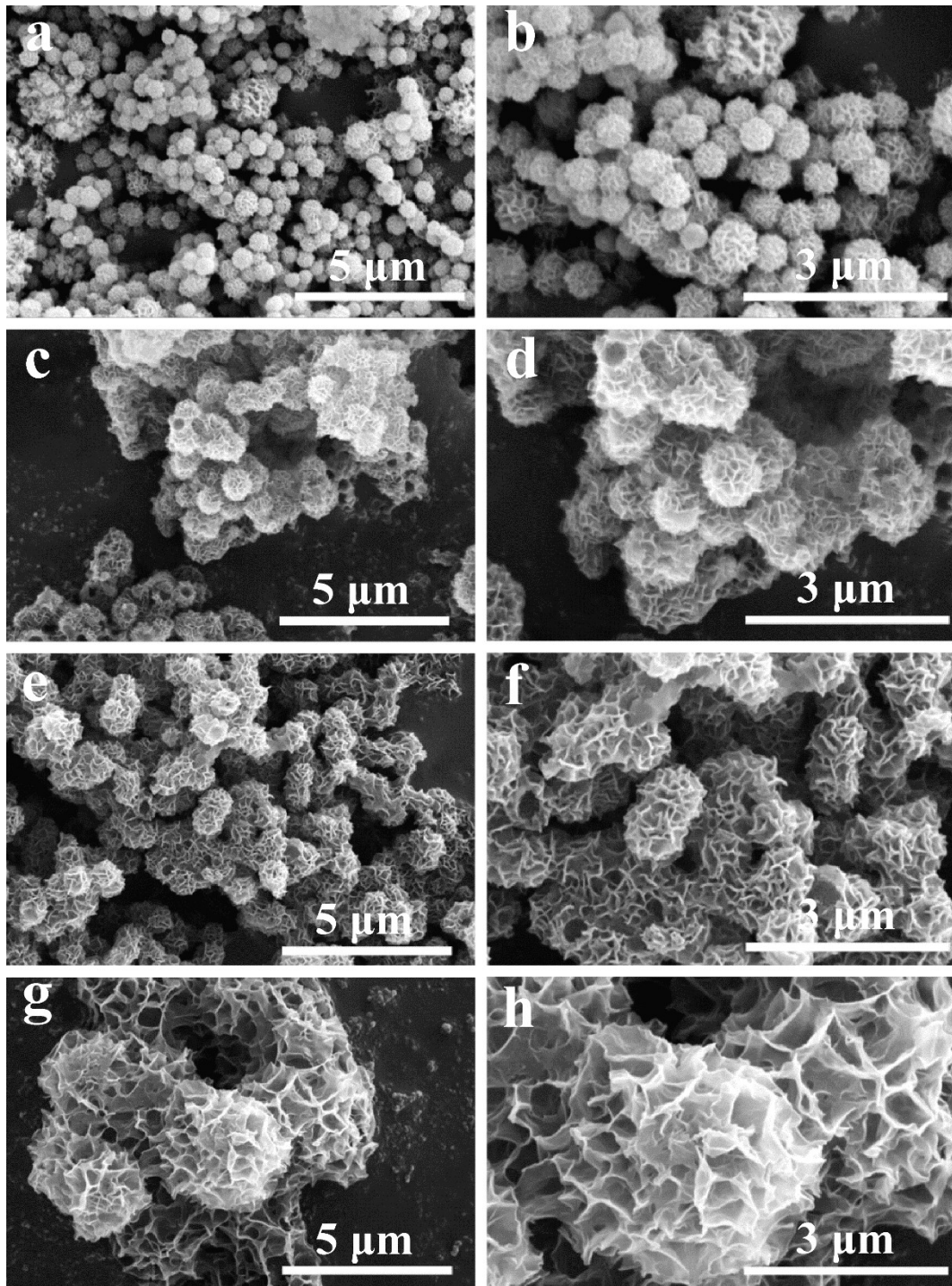
**Fig. S3.** SEM images of NiCoZn-CH prepared with different additions of $Zn^{2+}$ at different magnifications. **a-b**, $Ni_1Co_1Zn_0$-CH. **c-d**, $Ni_1Co_1Zn_{0.25}$-CH. **e-f**, $Ni_1Co_1Zn_{0.5}$-CH. **g-h**, $Ni_1Co_1Zn_1$-CH.

As shown in Fig. S3, the diameter of $Ni_1Co_1Zn_0$-CH is about 500 nm, $Ni_1Co_1Zn_{0.25}$-CH and $Ni_1Co_1Zn_{0.5}$-CH are about 800 nm, and $Ni_1Co_1Zn_1$-CH is about

3 μm. Flower-like nanospheres with interconnected two-dimensional nanosheets can provide a large specific surface area and abundant active sites for redox reactions, and facilitate the rapid diffusion of electrolyte ions. With the increase in $Zn^{2+}$ additions from 0 to 1 mmol, a clear change in nanosheets from small and thick to thin and large, and a gradual increase in the size of the nanospheres can be seen. However, excessive addition of $Zn^{2+}$ can destroy the flower-like structure and reduce the structural stability.

**Fig. S4.** SEM images of $Ni_1Co_1Zn_{0.25}$-CH prepared with different additions of urea at different magnifications. **a-b**, 0 mmol. **c-d**, 3 mmol. **e-f**, 9 mmol.

Fig. S4 displays SEM images of $Ni_1Co_1Zn_{0.25}$-CH prepared with different additions of urea at different magnifications. The results show that the nanosheets on the surface of nanospheres can be formed without the addiction of urea due to the hydrolysis reaction of NiCoZn-G nanospheres to produce hydroxide nanosheets (Fig. S4a-b). Fig. S4c-d shows the stacking and interweaving of the nanosheets into a flower-like structure and the nanosheets are uniform. As shown in Fig. S4e-f, spherical structures of NiCoZn-CH are destroyed and decomposed into stacked

nanosheets. The reason is that more carbonate ions and hydroxide ions are released at high urea concentrations, and NiCoZn-G solid spheres are greater etched, destroying the spherical structure.
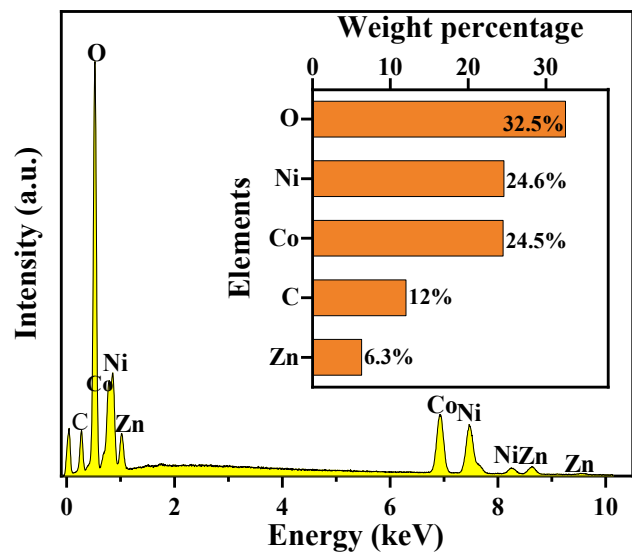
**Fig. S5.** EDS spectra of Ni1Co1Zn0.25-CH.

Fig. S5 shows the EDS spectra also indicate the presence of Ni, Co, Zn, C and O elements and the weight percentages of O, Ni, Co, C and Zn elements are 32.5%, 24.6%, 24.5%, 12% and 6.3%.
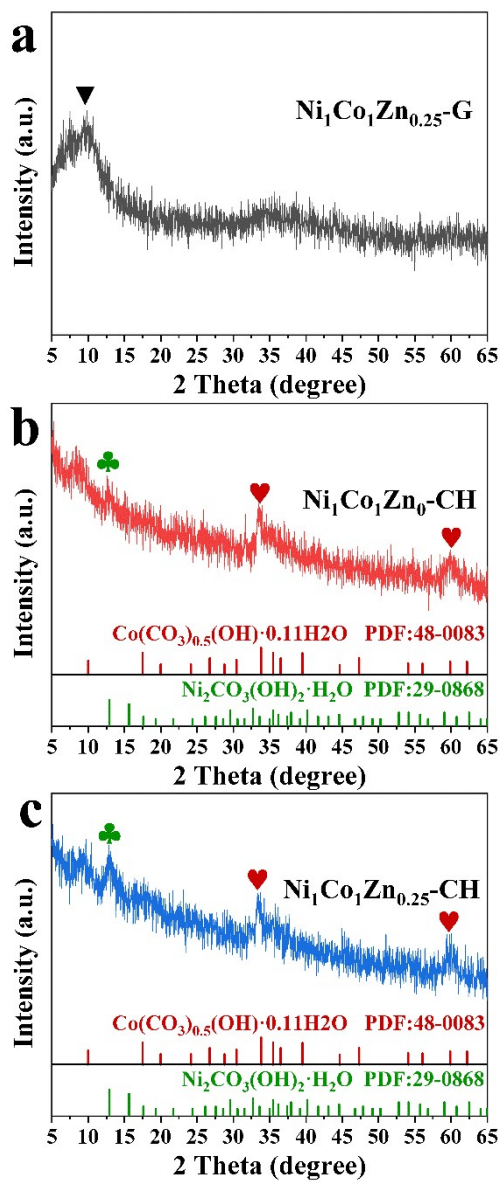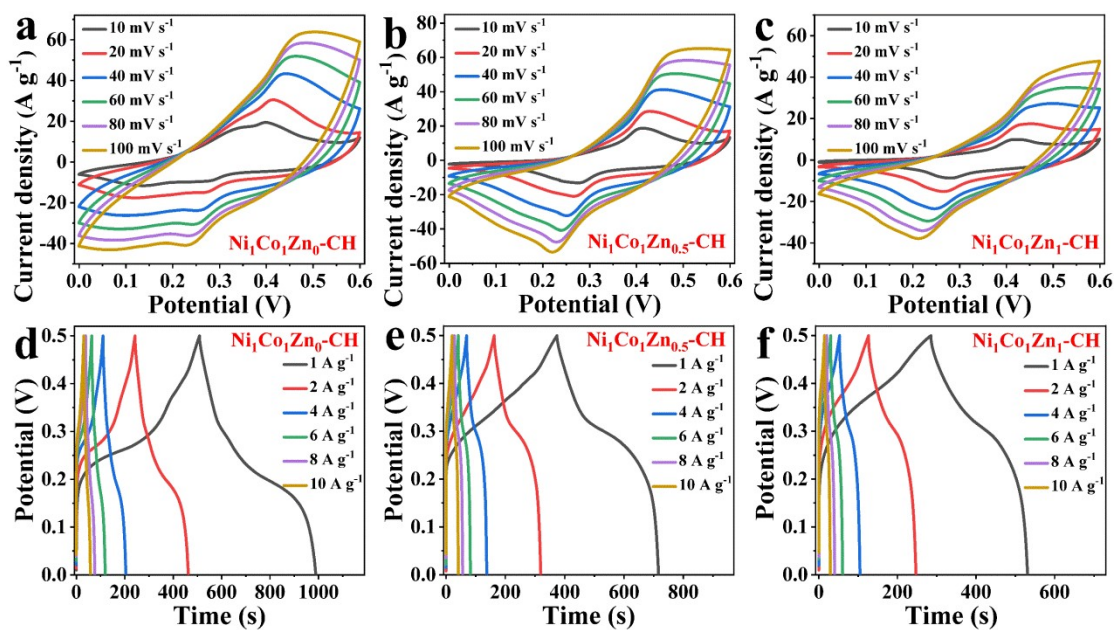
Fig. S6. The enlarged XRD patterns of $Ni_1Co_1Zn_{0.25}$-G, $Ni_1Co_1Zn_0$-CH and $Ni_1Co_1Zn_{0.25}$-CH.

**Fig. S7.** CV and GCD curves of other NiCoZn-CHs. **a-c**, CV curves at various scan rates from 10 to 100 mV s$^{-1}$. **d-f**, GCD curves at various current densities from 1 to 10 A g$^{-1}$.

Fig. S7 shows the CV and GCD curves of the other NiCoZn-CHs. Fig. S6a-c show the CV curves of the other NiCoZn-CHs at different additions of Zn$^{2+}$ at scan rates from 10 to 100 mV s$^{-1}$. There is no obvious change in the CV curve shape as the scan rate increases from 10 to 100 mV s$^{-1}$ due to the reversible redox reaction. Fig. S7e-f demonstrate the GCD curves of other NiCoZn-CHs at different current densities from 1 to 10 A g$^{-1}$. Ni$_1$Co$_1$Zn$_0$-CH, Ni$_1$Co$_1$Zn$_{0.5}$-CH, and Ni$_1$Co$_1$Zn$_1$-CH exhibit poor electrochemical properties.
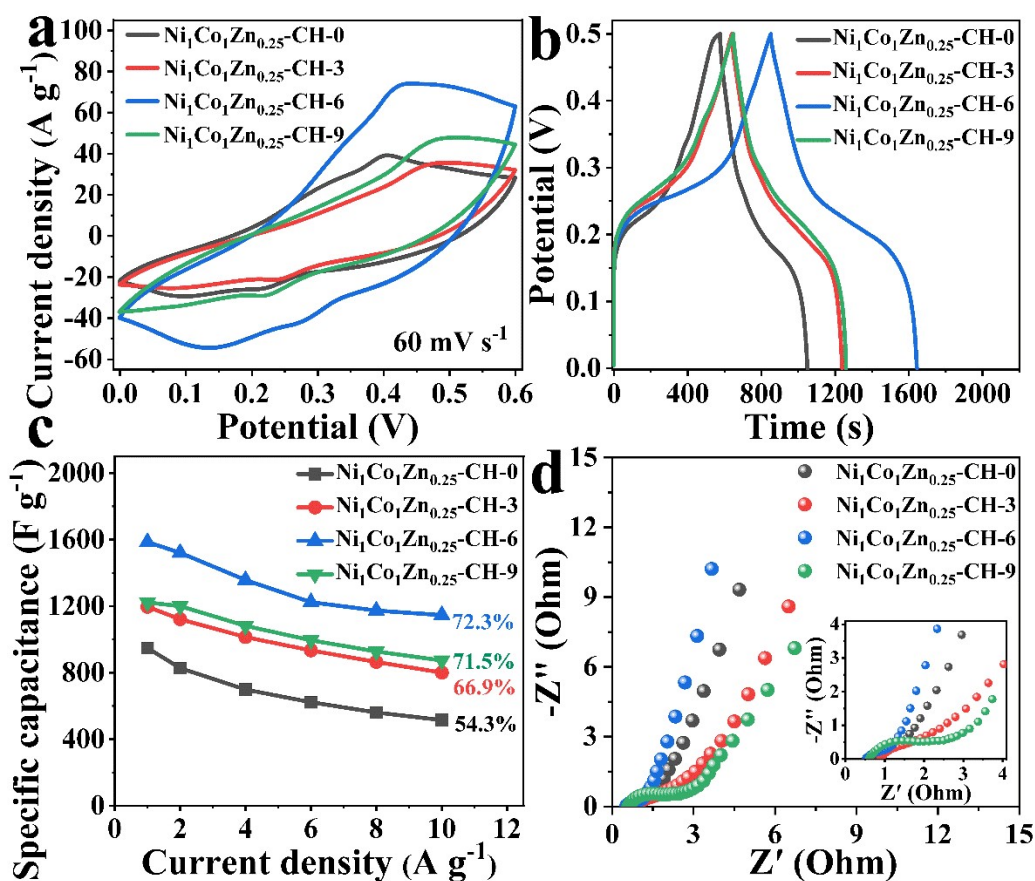
**Fig. S8.** Comparative electrochemical performance of $Ni_1Co_1Zn_{0.25}$-CH-X prepared with different additions of urea (X=0, 3, 6, 9 mmol). **a**, CV curves of $Ni_1Co_1Zn_{0.25}$-CH-X at 60 mV $s^{-1}$. **b**, GCD curves of $Ni_1Co_1Zn_{0.25}$-CH-X at 1 A $g^{-1}$. **c**, Variations of specific capacitance of $Ni_1Co_1Zn_{0.25}$-CH-X with different current densities. **d**, EIS curves of $Ni_1Co_1Zn_{0.25}$-CH-X. The inset is an enlarged diagram of the high-frequency range.

Fig. S8 shows the three-electrode electrochemical performance of $Ni_1Co_1Zn_{0.25}$-CH-X at different additions of urea (X=0, 3, 6, 9 mmol). All CV curves of these electrodes show clear redox peaks at 0-0.6 V at a scan rate of 60 mV $s^{-1}$(Fig. S8a). The GCD curves of these electrodes are plotted (Fig. S8b). The discharging time first increases and then decreases when the addition of urea increases, where $Ni_1Co_1Zn_{0.25}$-

CH-6 shows the longest discharge time. Furthermore, $Ni_1Co_1Zn_{0.25}$-CH-X (X=0, 3, 6, 9 mmol) show approximately 54.3%, 66.9%, 72.3%, and 71.5% specific capacitance retention at current densities from 1 to 10 A $g^{-1}$ (Fig. S8c). Fig. S8d shows the Nyquist plots of these electrodes. the $R_{ct}$ and $R_s$ values of $Ni_1Co_1Zn_{0.25}$-CH-6 is lower than the other electrodes. The above comparison shows that the electrochemical performance of NiCoZn-CH can be optimized by adjusting the parameters of urea addition.
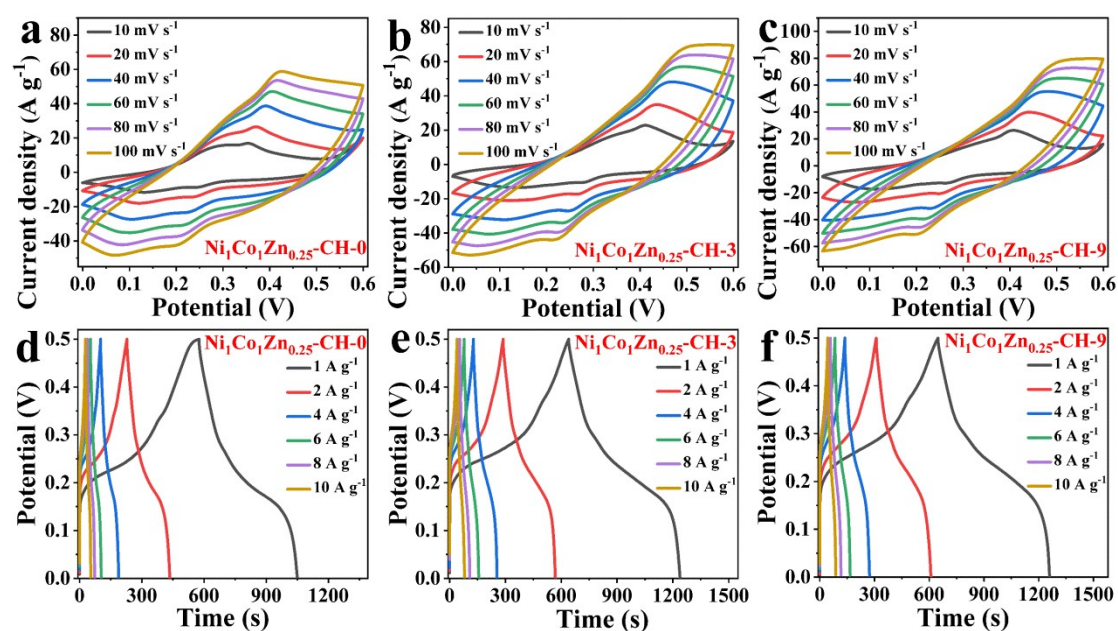
**Fig. S9.** CV and GCD curves of $Ni_1Co_1Zn_{0.25}$-CH-X prepared with different additions of urea (X=0, 3, 9 mmol). **a-c**, CV curves at various scan rates from 10 to 100 mV s$^{-1}$. **d-f**, GCD curves at various current densities from 1 to 10 A g$^{-1}$.

Fig S9 shows the CV and GCD curves for the other $Ni_1Co_1Zn_{0.25}$-CH-X prepared with different additions of urea (X=0, 3, 9 mmol). Fig. S9a-c show the CV curves of other $Ni_1Co_1Zn_{0.25}$-CH-X with different additions of urea at scan rates from 10 to 100 mV s$^{-1}$. As the scan rate increases from 10 to 100 mV s$^{-1}$, there is no significant change in the shape of the CV curves. Fig S9e-f indicate the GCD curves of the other $Ni_1Co_1Zn_{0.25}$-CH-X at different current densities from 1 to 10 A g$^{-1}$. $Ni_1Co_1Zn_{0.25}$-CH-0, $Ni_1Co_1Zn_{0.25}$-CH-3, and $Ni_1Co_1Zn_{0.25}$-CH-9 exhibit poor electrochemical properties.
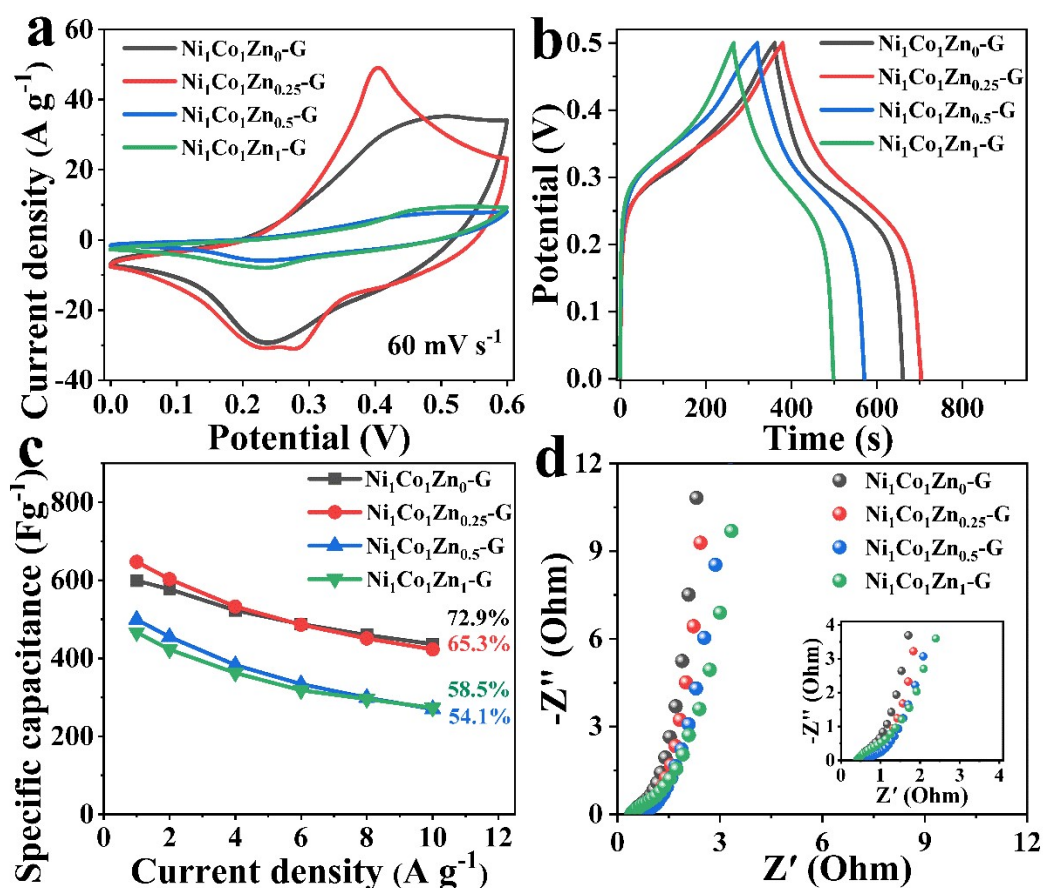
**Fig. S10.** Comparative electrochemical performance of NiCoZn-Gs. **a**, CV curves of NiCoZn-Gs at 60 mV s$^{-1}$. **b**, GCD curves of NiCoZn-Gs at 1 A g$^{-1}$. **c**, Variation of capacitances of NiCoZn-Gs at different current densities. **d**, EIS plots of NiCoZn-Gs, the inset is an enlarged plot of the high-frequency range.

Fig. S10 shows the three-electrode electrochemical performance of NiCoZn-Gs. All CV curves of these electrodes show clear redox peaks in the potential window of 0-0.6 V at 60 mV s$^{-1}$, with the integral area increasing and then decreasing when the Zn$^{2+}$ addition is increased (Fig. S10a). The GCD curves of these electrodes are plotted (Fig. S10b). When the Zn$^{2+}$ addition increases, the discharge time first increases and then decreases. In addition, Ni$_1$Co$_1$Zn$_{0.25}$-G shows the longest discharge time. The specific capacitance retentions of Ni$_1$Co$_1$Zn$_0$-G, Ni$_1$Co$_1$Zn$_{0.25}$-G, Ni$_1$Co$_1$Zn$_{0.5}$-G, and

$Ni_1Co_1Zn_1$-G are about 72.9%, 65.3%, 54.1% and 58.5% at 1 to 10 A $g^{-1}$ (Fig. S10c).

Fig. S10d shows the Nyquist plots of these electrodes. The $R_{ct}$ of $Ni_1Co_1Zn_{0.25}$-G is

lower than the other electrodes.
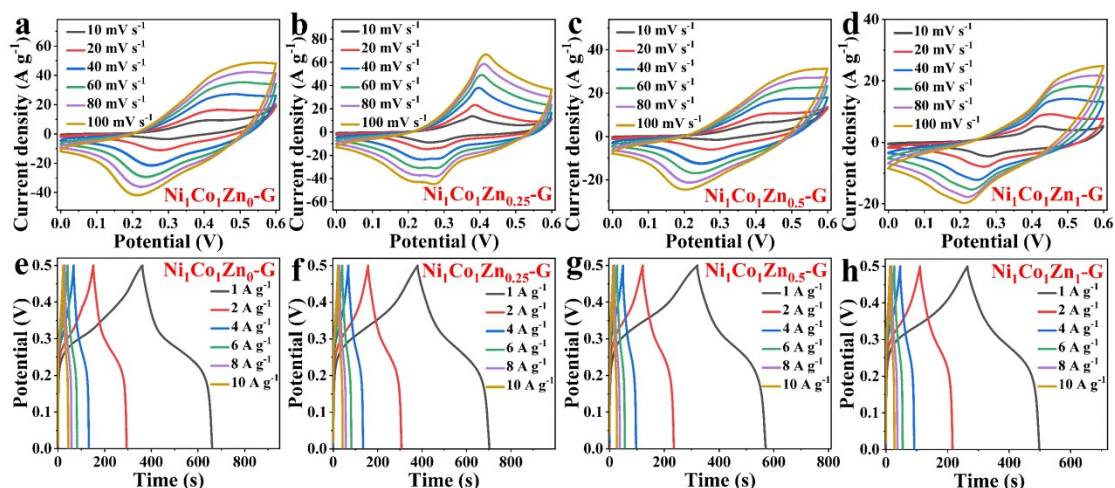
**Fig. S11.** CV and GCD curves of the NiCoZn-Gs. **a-c**, CV curves of NiCoZn-Gs at various scan rates from 10 to 100 mV s$^{-1}$. **d-f**, GCD curves of NiCoZn-Gs at various current densities from 1 to 10 A g$^{-1}$.

Fig. S11 shows the CV and GCD curves of NiCoZn-Gs. Fig. S11a-d show the CV curves for NiCoZn-G at different Zn$^{2+}$ additions at scan rates from 10 to 100 mV s$^{-1}$. Compared to Ni$_1$Co$_1$Zn$_0$-G, Ni$_1$Co$_1$Zn$_{0.5}$-G and Ni$_1$Co$_1$Zn$_1$-G, Ni$_1$Co$_1$Zn$_{0.25}$-G has the largest CV integral area. Due to the reversible redox reaction, there is no obvious change in the CV curve shape as the scan rates increase from 10 to 100 mV s$^{-1}$. Fig. S11e-h display the GCD curves of NiCoZn-Gs at 1 to 10 A g$^{-1}$, Ni$_1$Co$_1$Zn$_0$-G, Ni$_1$Co$_1$Zn$_{0.5}$-G, and Ni$_1$Co$_1$Zn$_1$-G exhibit shorter discharge time than Ni$_1$Co$_1$Zn$_{0.25}$-G. As shown in Fig. S9f, the specific capacitances of Ni$_1$Co$_1$Zn$_{0.25}$-G are 647.2 F g$^{-1}$, 603 F g$^{-1}$, 532.6 F g$^{-1}$, 486 F g$^{-1}$, 450.8 F g$^{-1}$ and 422.8 F g$^{-1}$ at 1-10 A g$^{-1}$, respectively. The above performance comparison shows that the electrochemical performance of the precursors can be optimized by adjusting the process parameters with the addition of Zn$^{2+}$.
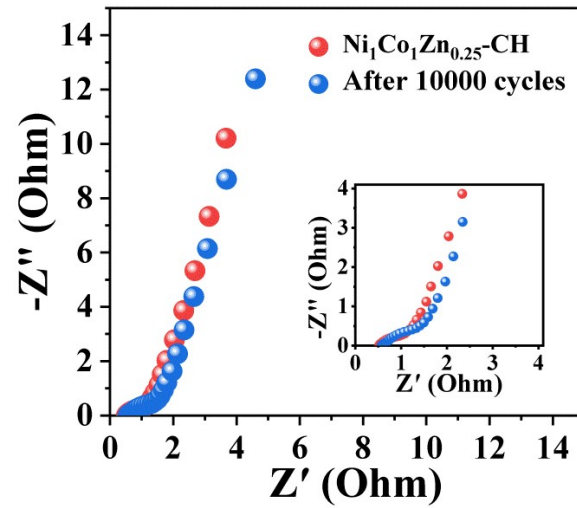
**Fig. S12.** EIS plots of $Ni_1Co_1Zn_{0.25}$-CH and $Ni_1Co_1Zn_{0.25}$-CH (after 10000 cycles), the inset is an enlarged plot of the high-frequency range.

Fig. S12 shows the Nyquist plots of $Ni_1Co_1Zn_{0.25}$-CH and $Ni_1Co_1Zn_{0.25}$-CH (after 10000 cycles). The $R_s$ and $R_{ct}$ of $Ni_1Co_1Zn_{0.25}$-OH are lower than $Ni_1Co_1Zn_{0.25}$-CH (after 10000 cycles).
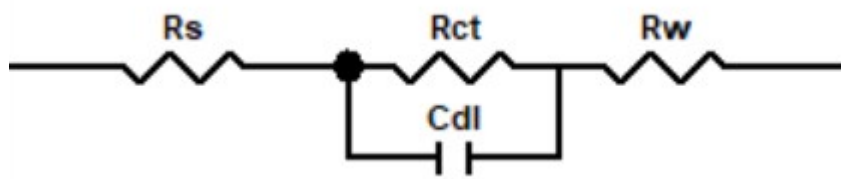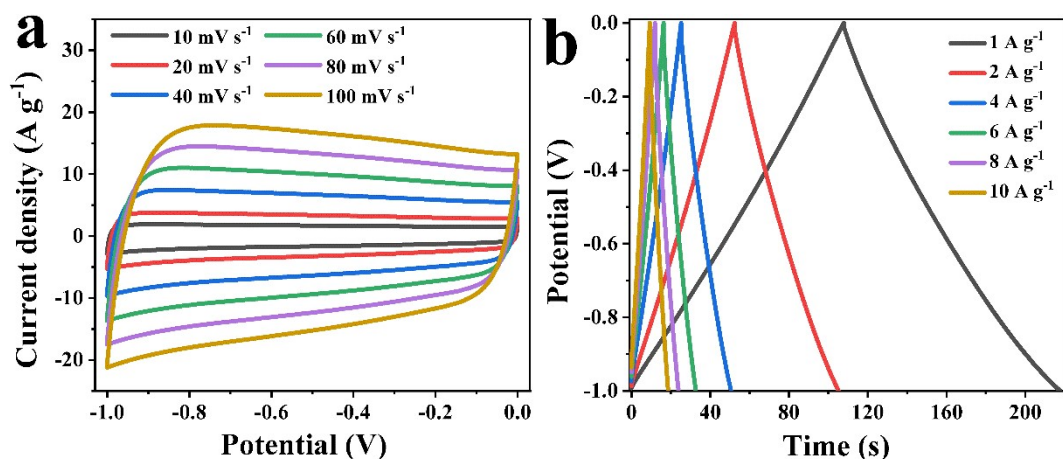
**Fig. S13.** Equivalent fitting circuit diagram

Rs: the equivalent series resistance

Rct: the charge transfer resistance

Rw: the diffusion resistance

Cdl: Double layered capacitance

**Fig. S14.** CV and GCD curves of AC. **a**, CV curves at various scan rates from 10 to 100 mV s$^{-1}$. **b**, GCD curves at various current densities from 1 to 10 A g$^{-1}$.

The electrochemical properties of the AC electrode are also investigated in a three-electrode configuration, as shown in Fig. S14. The rectangular CV curves at different scan rates and triangular GCD curves at different current densities can be seen, which are consistent with the capacitive characteristics of the electric double-layer energy storage mechanism. Based on the discharge curves of the GCD, the specific capacitances are calculated to be 109.95, 105.72, 100.76, 98.34, 95.76, and 93.3 F g$^{-1}$ for different current densities from 1 to 10 A g$^{-1}$.

**Table S1** The result of EIS data of different electrodes.

| Electrode | Impedance value (ohm) | | |
|---|---|---|---|
| | $R_s$ | $R_{ct}$ | $R_s+R_{ct}$ |
| $Ni_1Co_1Zn_0$-CH | 0.76 | 0.79 | 1.55 |
| $Ni_1Co_1Zn_{0.25}$-CH-6 | 0.52 | 0.57 | 1.09 |
| $Ni_1Co_1Zn_{0.25}$-CH (After 10000 cycles ) | 0.67 | 1.36 | 2.03 |
| $Ni_1Co_1Zn_{0.5}$-CH | 1.05 | 0.82 | 1.87 |
| $Ni_1Co_1Zn_1$-CH | 2.11 | 1.4 | 3.51 |
| $Ni_1Co_1Zn_{0.25}$-CH-0 | 0.64 | 0.9 | 1.54 |
| $Ni_1Co_1Zn_{0.25}$-CH-3 | 0.9 | 1.08 | 1.98 |
| $Ni_1Co_1Zn_{0.25}$-CH-9 | 0.61 | 1.55 | 2.16 |

**Table S2** The comparison of the electrochemical performance of various transition metal-based CHs.

| Nano-structure | Electrolyte | Specific capacitance | Rate performance | Cycling stability | Ref. |
|---|---|---|---|---|---|
| $Cu_xCo_{2-x}(CO_3)(OH)_2$ nanoplates | 6 M KOH | 789 $F \cdot g^{-1}$ at 1 $A \cdot g^{-1}$ | 49.6% (from 1 to 10 A g-1) | 77.5% over 3000 cycles at 5 $A \cdot g^{-1}$ | [S1] |
| MnNiCoCH/CF nanoneedles | 6 M KOH | 1440.52 $F \cdot g^{-1}$ at 1 $A \cdot g^{-1}$ | 70.76% (from 1 to 10 A $g^{-1}$) | 90.78% over 8000 cycles at 5 $A \cdot g^{-1}$ | [S2] |
| FeCoP nanosheets@Ni-Co carbonate hydroxide nanoneedles | 2 M KOH | 795.5 $C \cdot g^{-1}$ at 1 $A \cdot g^{-1}$ | 85.5% (from 1 to 20 A $g^{-1}$) | 89.7% over 5000 cycles at 5 $A \cdot g^{-1}$ | [S3] |
| Dandelion-like $(Ni_{0.89}Cu_{0.11})_2(OH)_2CO_3$ | 2 M KOH | 1017.3 $F \cdot g^{-1}$ at 1 $A \cdot g^{-1}$ | 61.4% (from 1 to 10 A $g^{-1}$) | 68.5% over 4000 cycles at 5 $A \cdot g^{-1}$ | [S4] |
| Mesoporous NiCuFeCoMn multistructure carbonate | 1 M KOH | 1241 $F \cdot g^{-1}$ at 1 $A \cdot g^{-1}$ | 26% (from 3 to 15 A $g^{-1}$) | 84.7% over 5000 cycles at 10 $A \cdot g^{-1}$ | [S5] |
| $Co(CO_3)_{0.5}(OH)/Ni_2(CO_3)(OH)_2$ nanobelts | 2 M KOH | 987 $F \cdot g^{-1}$ at 1 $A \cdot g^{-1}$ | 72.9% (from 1 to 30 A $g^{-1}$) | 82.9% over 2000 cycles at 10 $A \cdot g^{-1}$ | [S6] |
| Hybrid $NiCo(CO_3)(OH)_2$ nanowire/ $NiMn(CO_3)(OH)_2$ nanosheet | 1 M KOH | 1673.3 $F \cdot g^{-1}$ at 1 $A \cdot g^{-1}$ | 27.1% (from 3 to 15 A $g^{-1}$) | 82.1% over 5000 cycles at 5 $A \cdot g^{-1}$ | [S7] |
| $MoS_2$/NiCoHC | 2 M KOH | 1296 $F \cdot g^{-1}$ at 1 $A \cdot g^{-1}$ | 79.2% (from 1 to 10 A $g^{-1}$) | 81.5% over 5000 cycles at 5 $A \cdot g^{-1}$ | [S8] |
| Sunflower-like nickel– copper carbonate hydroxide | 2 M KOH | 1185.9 $F \cdot g^{-1}$ at 1 $A \cdot g^{-1}$ | 60.8% (from 1 to 10 A $g^{-1}$) | 93.1% over 5000 cycles at 2 $A \cdot g^{-1}$ | [S9] |
| Nickel carbonate hydroxide/nitrogen doped carbon quantum dots nanosheets | 3 M KOH | 727 $C \cdot g^{-1}$ at 1 $A \cdot g^{-1}$ | 66.4% (from 1 to 15 A $g^{-1}$) | 82.4% over 5000 cycles at 10 $A \cdot g^{-1}$ | [S10] |
| GCNF/PANI/$Ni_2(CO_3)(OH)_2$ | 3 M KOH | 1565 $F \cdot g^{-1}$ at 1 $A \cdot g^{-1}$ | 46.5% (from 1 to 20 A $g^{-1}$) | 80.8% over 4000 cycles at 5 $A \cdot g^{-1}$ | [S11] |
| **Flower-like $Ni_1Co_1Zn_{0.25}$-CH hollow nanospheres** | **6 M KOH** | **1585.2 F $g^{-1}$ at 1 A $g^{-1}$** | **72.3% (from 1 to 10 A $g^{-1}$)** | **87.9% over 10, 000 cycles at 10 $A \cdot g^{-1}$** | **This work** |

**Table S3** The comparison of the electrochemical performance of supercapacitors based on various CHs-based active materials.

| Supercapacitor device | Voltage (V) | Energy density (Wh kg$^{-1}$) | Power density (W kg$^{-1}$) | Cycling stability | Ref. |
|---|---|---|---|---|---|
| Cobalt hydroxide carbonate/GF//C-FP | 1.5 | 28 | 554 | 99.84% over 6000 cycles at 10 A·g$^{-1}$ | [S12] |
| NF@Co−CH@NiCoMn-CH//AC | 1.5 | 20.31 | 748.46 | 90.4% over 6000 cycles at 5 A·g$^{-1}$ | [S13] |
| Nickel-Copper carbonate hydroxide//AC | 1.6 | 32.7 | 359.9 | 88.8% over 5000 cycles at 2 A·g$^{-1}$ | [S9] |
| NiCo(CO$_3$)(OH)$_2$/NiMn(CO$_3$)(OH)$_2$ //Graphene | 1.6 | 27.2 | 702.7 | 89.4% over 5000 cycles at 5 A·g$^{-1}$ | [S7] |
| MoS$_2$/NiCoHC//AC | 1.5 | 16.4 | 375 | 65% over 5000 cycles at 5 A·g$^{-1}$ | [S8] |
| MnNiCo-CH/CF//AC | 1.5 | 30.04 | 749.97 | 83.86% over 8000 cycles at 5 A·g$^{-1}$ | [S2] |
| NiZnCoCH//AC | 1.5 | 29.6 | 375 | 80.2% over 5000 cycles at 4 A·g$^{-1}$ | [S14] |
| **Ni$_1$Co$_1$Zn$_{0.25}$-CH//AC** | **1.6** | **333.7** | **400** | **99.9% over 15000 cycles at 10 A·g$^{-1}$** | **This work** |

# References

[S1] S. Liu, K. S. Hui, K. N. Hui, V. V. Jadhav, Q. X. Xia, J. M. Yun, Y. R. Cho, R. S. Mane and K. H. Kim, *Electrochimica Acta*, 2016, **188**, 898–908.

[S2] X. Cao, Y. Liu, Y. Zhong, L. Cui, A. Zhang, J. M. Razal, W. Yang and J. Liu, *Journal of Materials Chemistry A*, 2020, **8**, 1837–1848.

[S3] L. Wan, Y. Wang, Y. Zhang, C. Du, J. Chen, Z. Tian and M. Xie, *Chemical Engineering Journal*, 2021, **415**, 128995.

[S4] P. W. Yuan, S. H. Guo, S. Q. Gao, J. Wang, W. Q. Chen, M. Li, K. Y. Ma, N. Wang, F. Liu and J. P. Cheng, *Journal of Alloys and Compounds*, 2019, **780**, 147–155.

[S5] A. Verma, K. H. Kim, S. Mathur and D. Lee, *JOURNAL OF ALLOYS AND COMPOUNDS*, 2022, **922**, 166222.

[S6] G. Zhang, P. Qin, R. Nasser, S. Li, P. Chen and J.-M. Song, *CHEMICAL ENGINEERING JOURNAL*, 2020, **387,** 124029.

[S7] D. Lee, K. S. Kim, J. M. Yun, S.-Y. Yoon, S. Mathur, H.-C. Shin and K. H. Kim, *Journal of Alloys and Compounds*, 2019, **789**, 119–128.

[S8] A. Y. Chen, H. H. Liu, P. Qi, X. F. Xie, M. T. Wang and X. Y. Wang, *Journal of Alloys and Compounds*, 2021, **864**, 158144.

[S9] A. Bera, A. K. Das, A. Maitra, R. Bera, S. K. Karan, S. Paria, L. Halder, S. K. Si and B. B. Khatua, *Chemical Engineering Journal*, 2018, **343**, 44–53.

[S10] Z. Ji, D. Ma, W. Dai, K. Liu, X. Shen, G. Zhu, Y. Nie, D. Pasang and A. Yuan, *Journal of Colloid and Interface Science*, 2021, **590**, 614–621.

[S11]    Y. Zhao, Y. Wang, Y. Huang, W. Liu, J. Hu, J. Zheng and L. Wu, *Journal of Colloid and Interface Science*, 2023, **630**, 444–451.

[S12]    T. M. Masikhwa, D. Y. Momodu, K. O. Oyedotun, A. A. Mirghni, N. M. Ndiaye and N. Manyala, *Journal of Alloys and Compounds*, 2018, **769**, 376–386.

[S13]    Y. Zhong, X. Cao, Y. Liu, L. Cui and J. Liu, *Journal of Colloid and Interface Science*, 2021, **581**, 11–20.

[S14]    H. Gu, Q. Zhong, Y. Zeng, S. Zhang and Y. Bu, *Journal of Colloid and Interface Science*, 2020, **573**, 299–306.